Available online at www.sciencedirect.com
ScienceDirect
Metamaterials 3 (2009) 10–27
Metamaterials
www.elsevier.com/locate/metmat

Invited paper

Metamaterial made of paired planar conductors: Particle resonances, phenomena and properties

G. Donzelli [a,d], A. Vallecchi [a], F. Capolino [b,*], A. Schuchinsky [c]

[a] *Department of Information Engineering, University of Siena, Via Roma 56, 53100 Siena, Italy*
[b] *Department of Electrical Engineering and Computer Science, University of California, Irvine, CA 92697, USA*
[c] *Queen's University Belfast, Belfast BT3 9DT, United Kingdom*
[d] *Now with Altran Italia, 20154 Milano, Italy*

Received 4 April 2008; received in revised form 11 November 2008; accepted 16 December 2008
Available online 24 January 2009

Abstract

The properties and characteristics of a recently proposed anisotropic metamaterial based upon layered arrays of tightly coupled pairs of "dogbone" shaped stripe conductors have been explored in detail. It has been found that a metamaterial composed of such stacked layers exhibits artificial magnetism and may support backward wave propagation. The equivalent network models of the constitutive conductor pairs arranged in the periodic array have been devised and applied to the identification of the specific types of resonances, and to the analysis of their contribution into the effective dielectric and magnetic properties of the artificial medium. The proposed "dogbone" configuration of conductor pairs has the advantage of being entirely realizable and assemblable in planar technology. It also appears more prospective than simple cut-wire or metal-plate pairs because the additional geometrical parameters provide an efficient control of separation between the electric and magnetic resonances that, in turn, makes it possible to obtain a fairly broadband left-handed behaviour of the structure at low frequencies.

Keywords: Artificial magnetism; Coupled conductors; Dogbones; Metamaterials; Microwaves; Negative refractive index; Planar technology; Transmission lines

1. Introduction

Artificial magnetism is considered as one of the major attributes of metamaterials along with negative refractive index (NRI). Periodic arrays of magnetic dipoles emulated by resonant loops are often realized with the aid of split ring resonators (SRRs) [1–3]. Combined with wires, SRRs are used as the constituent particles of artificial media in which effective NRI can be observed for plane waves of fixed polarization incident at certain angles [4,5]. In numerous publications, such media are described as materials with negative permeability and permittivity.

At optical frequencies, materials made of pairs of nanorods have been suggested in Ref. [6] to create current loops resonating in the transmission line mode, i.e., each pair of rods constitutes a waveguide resonator comprised of two conductors. It has been shown that a pair of coupled conducting wires may possess two types of resonances, named electric and magnetic resonances, and could represent the basic building block of a NRI medium. Although the SRRs and coupled rods have demonstrated feasibility of producing the NRI response of the medium, search of novel physical structures for

* Corresponding author.
E-mail address: capolino@dii.unisi.it (F. Capolino).

1873-1988/$ – see front matter © 2009 Published by Elsevier B.V.
doi:10.1016/j.metmat.2008.12.001

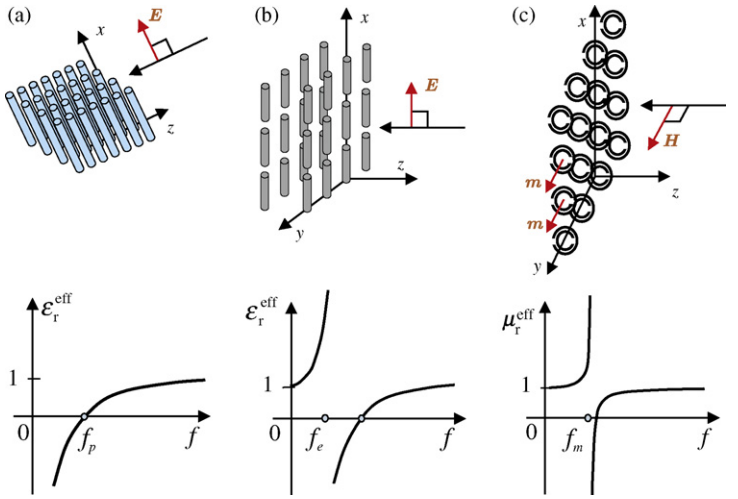

Fig. 1. Wire medium (a) and cut-wire medium (b). The frequency dependent effective permittivity at the shown polarization of the incident electric field is characterised by a plasma-like resonance frequency f_p and by an electric resonance frequency f_e associated with a standard stop band of FSS. (c) One layer of SRRs, polarization of incident magnetic field and induced magnetic moments m at the magnetic resonance f_m. The layer of SRR is in the x–y plane, the SRRs are aligned parallel to the x–z plane.

the constituent particles still remains an acute problem. Alternative geometries based on the same principles have been proposed for microwave frequencies in Refs. [7–10], and the planar arrangement of the "dogbone" shaped tightly coupled conductor stripes [11–14] is the subject of this paper.

In this work we perform a detailed study of the resonances in the dogbone structure, their types and dependences on the geometrical parameters. We also propose an accurate transmission line model of a single dogbone particle, which enables us to predict the magnetic resonance frequencies and provides simple approximate formulas useful for design purposes. A single layer of dogbone pairs is analyzed first. Then multilayered structures are investigated, and we show the existence of a frequency band where artificial magnetism and backward wave propagation exist in the periodic arrangements with lattice constants significantly smaller than the wavelength. Using the simple algorithm based on the observation of the transmitted wave phase (see, e.g. [15,16]), the metamaterial backward wave propagation characteristics are retrieved from the scattering parameters of a wave normally incident on a few stacked layers of arrayed dogbone pairs. The metamaterial properties are retrieved also by observing the Bloch propagation constant between layers that clearly identifies the backward wave propagation bands. We address the readers to [17] for a comprehensive discussion of metamaterial homogenization. The results of these analyses provide the theoretical demonstration that the dogbone pair structure can exhibit a fairly broadband NRI behavior at low frequencies.

The paper is organized as follows. In Section 2 we introduce the main concepts and recall the effective medium description of metamaterials made of wires, cut-wires and SRRs. In Section 3 we carry out an extensive parametric analysis and investigate the transmission properties of a single layer of dogbone pairs on a dielectric substrate and in free-space. In Section 4, a transmission line model is introduced and applied to prediction of the magnetic resonance frequency. In Section 5 we show that metamaterials composed of several layers of dogbone pairs may exhibit backward wave propagation. Major findings are summarized in Section 6.

2. Background. Electric and magnetic resonances in wire and SRR materials

The wire medium, the cut-wire medium, and the periodic array of SRRs shown in Fig. 1 represent the canonical types of metamaterials, which are usually characterized by effective permittivity and permeability expressed in terms of the associated plasma frequency, and electric and magnetic resonances. Since the 50's and 60's the wire medium shown in Fig. 1(a) has been described for an incident electric field parallel to the wires as an artificial dielectric [18–20] with an isotropic effective plasma-like relative permittivity $\varepsilon_r^{eff} = 1 - f_P^2/f^2$, where f is the signal frequency, f_p

is the plasma frequency which depends on the wire diameter and interspacing, see [21–24] (such medium is assumed to be lossless, which is a reasonable approximation at microwave frequencies). Spatial dispersion should be additionally taken into account when the waves travel at a slant angle to the wire axes [25,26]. For waves propagating normally to the wires, and in the absence of losses, a homogenized wire medium exhibits negative effective permittivity at $f<f_p$ (see Fig. 1(a)), and such an artificial dielectric is opaque, whereas for $f>f_p$ the effective permittivity is positive and the artificial dielectric is translucent. When the wires are cut, see Fig. 1(b), the wire medium is still described by an effective permittivity but ε_r has different frequency dependence, as explained in Ref. [24].

The medium made of SRRs, Fig. 1(c), can be also described by a homogeneous effective permeability which is represented in the general form $\mu_r^{eff} = 1 - Af^2/(f^2 - f_m^2 - j\Gamma f)$ where f_m and Γ stand for the resonance and damping frequencies, respectively, and A denotes the resonance amplitude [1,27].

When wires and SRRs are combined in a single structure, the resulting composite medium may exhibit NRI [4,5] entailed by both effective permittivity and permeability being negative, and thus supports backward wave propagation. Indeed, as shown in Fig. 1(c), the SRRs are periodically offset in the x–y plane whilst each SRR lies in the x–z plane, orthogonal to the incident magnetic field H. However, physical realization of such material involves a complex manufacturing process. Though it is not impractical at microwaves, the fabrication and assembling of the SRRs and wire arrays for THz and optical frequencies, where the most exciting applications are expected, face major challenges. In order to alleviate these difficulties, an alternative arrangement of the constitutive resonant particles fully compatible with the planar technology is proposed in this paper to realize composite metamaterials very well-suited for applications at microwave and millimeter-wave frequencies and also having the potential for expanding to the optical range.

This investigation has been inspired by some recent works [6–10] which suggested that pairs of finite length wires could be used as magnetic resonators instead of SRRs. The wires could also give simultaneously a negative permittivity in the same frequency range and therefore a NRI, without the need for continuous wires. However, achieving simultaneously the negative permeability and permittivity with pairs of metallic wires is subject to some restrictions, cf. [7,11]. Indeed, the difficulty of obtaining NRI with cut-wire pairs rests in the fact that the electric resonance is generally stronger and wider than the magnetic one. Thus, if the electric resonance of the cut-wires is well above the magnetic resonance frequency, simultaneous negative permittivity and permeability cannot be attained. As a consequence, one usually needs to locate the magnetic resonance within the negative permittivity region (unless the region of negative permeability can be made wide enough to overlap, at least partially, the negative permittivity region). However, in a simple cut-wire pair, an independent tuning of these two resonances is impossible because the frequencies of both the electric and the magnetic resonances are controlled by a single geometrical parameter—the length of the wires (both frequencies are approximately proportional to the inverse of wire length) [8].

A convenient approach to realize NRI response of short-strip pairs is to combine them with continuous wires. This provides a large negative permittivity band due to the plasmonic response of the wire medium, and one can exploit only the negative effective permeability produced by the strip pairs [7].

Another possibility to accomplish an independent variation of the electric and magnetic resonances is to strengthen the interaction of the pairs in the adjacent unit cells along the electric field direction. This can be achieved by reducing the distance between the contiguous pairs or increasing the strip widths at their ends [11]. In general, an additional inter-pair capacitance, resulting from this enhanced interaction, influences the electric resonance frequency stronger than the magnetic one. For very closely spaced conductor pairs, the magnetic resonance is substantially affected by the capacitance between the top and bottom conductors in the pair. When the spacing between the top and bottom conductors in the pair is comparable with the distance between the contiguous pairs, the capacitive coupling between the pairs has strong impact on the magnetic resonance, as shown in this paper. Thus modification of the cut-wire topology toward the dogbone shape, whose lateral arms contribute to both the self- and mutual capacitances, provides a new means for controlling the locations of the electric and magnetic resonance frequencies, so as to make them even completely overlap and display the NRI behaviour over a broad frequency band [11].

It is necessary to note that the concept of strong coupling inside the conductor pairs also underlies operation of the so-called fishnet structure, which was originally introduced in Ref. [28]. Indeed, the fishnet design can be seen as the evolution of the strip-pairs and continuous wires [7] when the width of the strips is increased until they join the infinite wires [8] thus producing a continuous connected mesh. The paired fishnets also provide the additional parameters to control the positions of electric

and magnetic resonances, and the fishnet proved to be an effective structure for implementation of NRI characteristics [28–32]. However, fully isotropic and deep sub-wavelength scale designs (required, for example, for the full exploitation of the superlensing capabilities of metamaterials) is difficult to achieve with the fishnet configuration which has a unit cell size typically of an order of half a wavelength and whose optimal operation has been demonstrated for normal incidence.

The arrays of dogbone shaped conductors discussed in this paper are free from the aforementioned limitations and exhibit the attractive feature of a reduced unit cell size, due to the additional capacitive loading provided by the dogbone lateral arms. Furthermore, the dogbone pairs represent the basic blocks of more intricate arrangements which can handle arbitrary polarizations and oblique incident fields. For example, a completely symmetrical configuration is realized by simply combining two orthogonal dogbone particles to form tightly coupled Jerusalem crosses, which are invariant to linear polarization of a wave at normal incidence. Therefore all the results obtained in this paper for the dogbone pairs at a single incident polarization can be readily extended to the Jerusalem cross pairs, and the polarization-dependent NRI behaviour of the dogbones enables an isotropic effective NRI response of the Jerusalem crosses [33].

Finally, it is noteworthy that the NRI properties of the dogbone pairs are theoretically demonstrated in this paper for microwave frequencies. But the ease of fabrication of this kind of planar metamaterial, using a single dielectric sheet, is expected to facilitate also its scaling to THz and optical frequencies, provided that the change of the metal properties from lossy conductors at microwave frequencies to lossy dielectrics with negative permittivity in the THz range is adequately taken into account. Indeed, these dogbone structures present the same level of fabrication complexity as simple cut-wire pairs, which have already been manufactured and studied experimentally at optical wavelengths [6].

3. Metamaterial in planar technology: the "dogbone" particle and its properties

Objective of this work is to investigate a planar periodic structure which has the potential to act as an effective NRI medium. A parametric study has been performed to gain physical insight into the mechanisms of the resonance formation and field interactions in the planar doubly periodic arrays of resonant particles made of pairs of tightly coupled dogbone shaped conductors. The properties of such structures illuminated by a normally incident (along the z-axis) plane wave, as shown in Fig. 2, are discussed for different geometries of the unit cells. The incident electric field is polarized along the x-direction, parallel to the central main segment of the dogbone. In this paper we aim at investigating the basic properties of dogbone-based arrays such as resonance frequency locations and NRI possibilities, and therefore conductors are assumed lossless, which is a reasonable approximation at microwave frequencies.

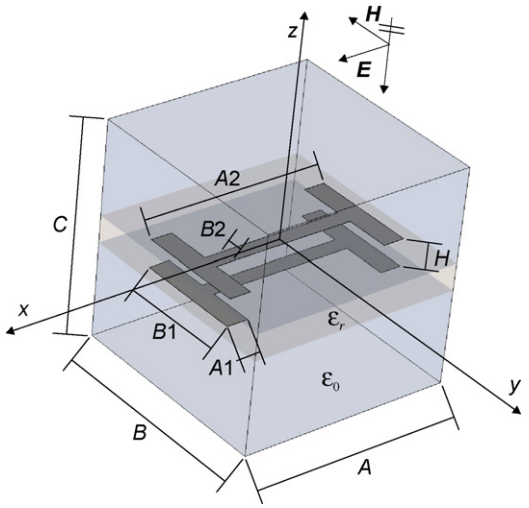

Fig. 2. Dogbone particle made of a pair of tightly coupled planar conductors separated by an insulating dielectric layer. The incident electric field is polarized along the x-direction.

3.1. Dogbone pair of conductors separated by a dielectric layer

The properties of an array formed by the dogbone conductor pairs shown in Fig. 2 are investigated through simulations of the transmission coefficient $|T|$ for a set of structure parameters which are varied one at a time. The dogbone pairs are assumed to be formed by infinitesimally thin perfect electric conductors. The simulation results at the following default values (in mm): $A = B = 7.5$, $C = 8$, $B1 = 4$, $A2 = 7.4$, $B2 = 0.8$, $A1 = 1$, $H = 0.2$, $\varepsilon_r = 16$, are presented in Figs. 3–11 and discussed in this section. The main purpose of this detailed analysis is to identify and evaluate the impact of specific geometric features on the array resonance characteristics.

At first, the cell size A (the period) along the x-direction was varied. The plots in Fig. 3(a) illustrate the first two resonances in this structure. In order to assess the accuracy of the obtained results, the structure with the default parameters was simulated using both Ansoft HFSS and CST Microwave Studio, and the two sets of simulated data have shown a good agree-

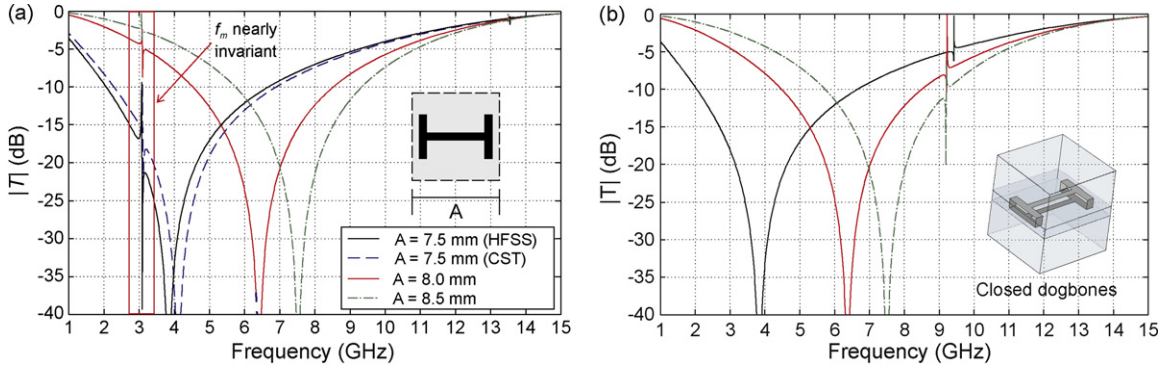

Fig. 3. Transmission coefficient vs. size A of a unit cell in a doubly periodic planar array composed of dogbone paired conductors (a) shown in Fig. 2, and (b) conductors with short-circuited "arms" (see insert). The electric resonances for both the structures are at $f_e \approx 3.9$, 6.4, 7.5 GHz, whereas the magnetic resonance at $f_m \approx 3.1$ GHz in case (a) is suppressed when the lateral arms of the dogbones are short-circuited in case (b).

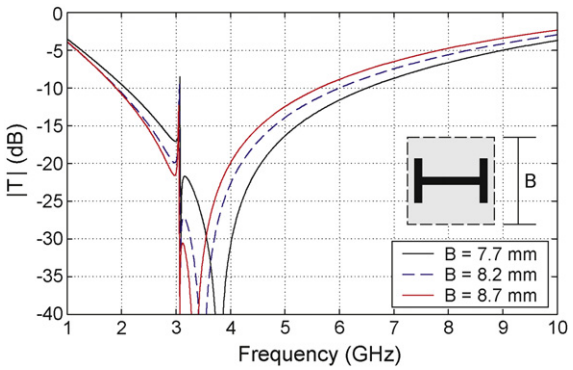

Fig. 4. Transmission coefficient vs. unit cell size B for a doubly periodic planar array composed of dogbone pairs shown in Fig. 2. The electric resonance is at $f_e \approx 3$–4 GHz. The magnetic resonance is at $f_m \approx 3.1$ GHz.

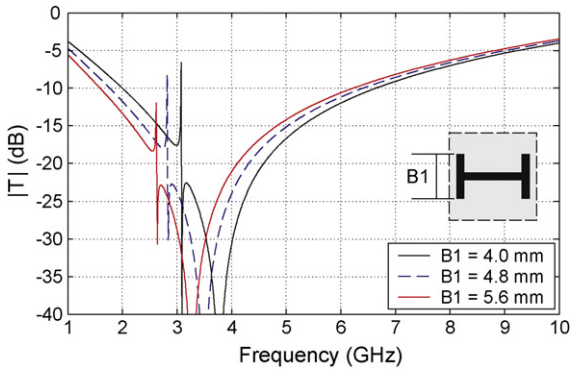

Fig. 6. Transmission coefficient vs. lateral arm length $B1$ in a doubly periodic planar array composed of the dogbone pairs shown in Fig. 2. The electric resonance varies in the range $f_e \approx 3.2$–3.9 GHz. The magnetic resonance varies in the range $f_m \approx 2.5$–3.1 GHz.

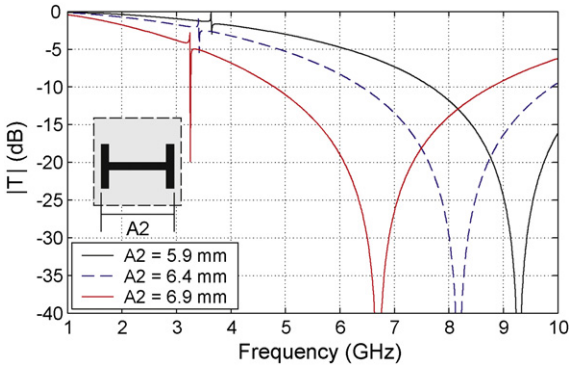

Fig. 5. Transmission coefficient vs. dogbone length $A2$ in a doubly periodic planar array composed of the dogbone pairs shown in Fig. 2. The electric resonances are at $f_e \approx 6.8$, 8.2, 9.3 GHz. The magnetic resonances f_m vary between 3 and 4 GHz.

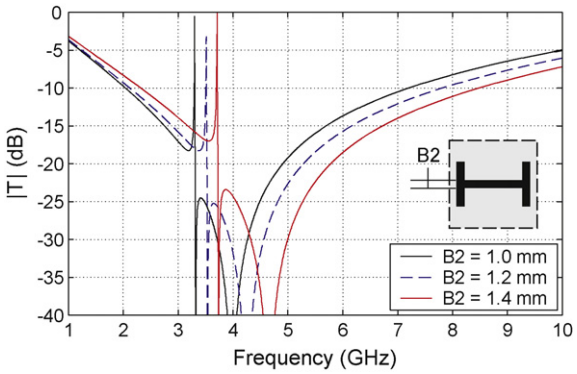

Fig. 7. Transmission coefficient vs. width $B2$ of the dogbone central part in a doubly periodic planar array composed of the dogbone pairs shown in Fig. 2. The electric resonance varies in the range $f_e \approx 4$–4.6 GHz. The magnetic resonance varies in the range $f_m \approx 3.3$–3.7 GHz.

ment. The lowest resonance at $f \approx 3.1$ GHz appears to be practically unaffected by variations of A, thus indicating that the fields are confined to the close proximity of the dogbone pair and are loosely coupled to the adjacent cells. This resonance, usually referred to as the *magnetic resonance*, is of particular interest in this paper as elaborated later. Its frequency f_m mainly depends on the dogbone particle dimensions and is associated with the so-called transmission line (TL) mode which creates an equivalent magnetic dipole moment. The other resonance, denoted as *electric resonance*, is associated with a dipole-like *symmetric mode*, which creates an electric dipole moment. It exhibits a much wider stopband, and its frequency f_e ($\approx$3.9, 6.4, 7.5 GHz) strongly depends on the lattice constant A. This implies that the electric resonance is rendered by the capacitive coupling between the dogbone particles in the adjacent cells, similarly to that in the capacitive type of frequency selective surfaces (FSS), for example, of dipoles or Jerusalem crosses [34].

In order to verify such a designation of the resonant modes, the same dogbone particle has been simulated when its lateral arms were short-circuited, see Fig. 3(b). Comparison of the corresponding plots in Fig. 3(a) and (b) shows that the magnetic resonance at $f_m \approx 3.1$ GHz is suppressed in the structure with the short-circuited arms whilst the electric resonances at f_e remain nearly unchanged. This confirms that the resonance at $f_m \approx 3.1$ GHz in Fig. 3(a) is indeed of the magnetic type, which corresponds to the *antisymmetric mode* with oppositely directed currents flowing on the top and bottom conductors of each dogbone pair, and these currents are strongly affected when the arms are short-circuited. Conversely, the electric resonance at f_e is weakly perturbed by the short circuits because it is produced by a symmetric mode whose currents flow in the same direction on both the top and bottom conductors of the dogbone particle.

The proposed interpretation of the resonance modes is also supported by the simulation results for variable cell size B (the period along the y-axis). Fig. 4 shows that the magnetic resonance at $f_m \approx 3.1$ GHz remains unchanged while the electric resonance slightly shifts in the range $f_e \approx 3.4$–3.9 GHz because the particle mutual coupling in y-direction is weakly influenced by the size B as long as $(B - B1) \gg H$.

Once the resonance types have been identified and the lattice constant effect is understood, we can evaluate how the resonance frequencies are affected by the geometry of the dogbone itself. The dogbone length $A2$ along the x-direction was varied first, and its effect is illustrated in Fig. 5 at the fixed cell size A. Both magnetic and electric resonances are displaced now. A smaller shift of the magnetic resonance indicates that its frequency is attributed to the incremental increase of the total coupling between top and bottom conductors and self-inductance of the dogbone particles. This effect will be further discussed in connection with variations of other dimensions and later interpreted with the aid of the TL model described in Section 4. The electric resonance f_e proved to be more sensitive to the size $A2$. However it is necessary to emphasize that the f_e shift is predominantly determined by the change of capacitive coupling between the adjacent cells, and to a smaller degree by the dogbone length. Therefore, when increasing $A2$, not only does the electrical length increase (causing a decrease of f_m and f_e), but also the capacitive coupling between contiguous cells (inversely proportional to $A - A2$) increases, and this latter effect is the main cause of the f_e shift towards lower frequencies. Indeed, comparison of Figs. 3 and 5 shows that the rate of f_e changes with $A2$ and A is nearly the same (cf. $A = 8$ and 8.5 mm and $A2 = 6.4$ and 6.9 mm).

As mentioned in Section 2, the lateral arms of the dogbone particles represent one of the major distinctive features of this structure. Therefore the effect of the dogbone "arms" length $B1$ should be analyzed to gain insight into the unique properties of the dogbone particles. The simulation results in Fig. 6 demonstrate that both the magnetic and electric resonances shift towards lower frequencies at larger $B1$. However different mechanisms appear to be responsible for this phenomenon. The lower frequency of the magnetic resonance at the longer arms' length $B1$ is associated with the increase of the capacitance between the top and bottom parts of the dogbone arms (similarly to the case of $A2$ variations in Fig. 5). Indeed, it is evident now and will be further illustrated in the rest of this section that the *magnetic* resonance can be attributed to the resonant TL mode (also called *antisymmetric mode*) as elaborated in Section 4. The *electric* resonance, on the other hand, is governed by the coupling between the particles in the adjacent cells similarly to that in the dipole-based FSS [24]. Therefore incremental increase of $B1$ has about the same impact on f_m as on f_e, though the former phenomenon is mainly associated with the dogbone elongation, whilst the latter is caused by a larger capacitance to the adjacent cells.

The discussion of the dogbone particle resonances has so far been concerned with the effects of the dogbone arm lengths and the unit cell size. While being instrumental in identifying the resonance types and features, we could not distinguish the coupling mechanisms involved. In order to gain deeper insight in the nature of these resonance interactions, the effect of the stripe widths $B2$ and $A1$ should be assessed.

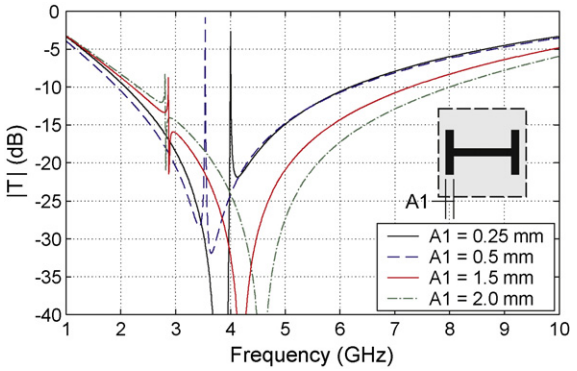

Fig. 8. Transmission coefficient vs. lateral arm width $A1$ in a doubly periodic planar array composed of the dogbone pairs shown in Fig. 2. The electric resonance varies in the range $f_e \approx 3.5$–4.5 GHz. The magnetic resonance varies in the range $f_m \approx 2.8$–4 GHz.

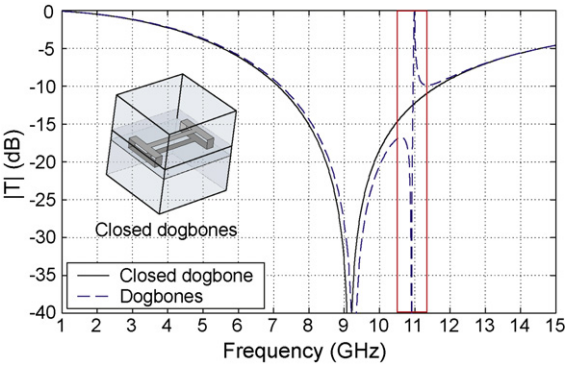

Fig. 10. Transmission coefficients for the doubly periodic planar arrays of dogbone pairs with isolated conductors (Fig. 2) and short-circuited arms (closed dogbones in insert) in *free-space*. The electric resonance occurs at $f_e \approx 9.1$ GHz, and the magnetic resonance is at $f_m \approx 11$ GHz.

The characteristics simulated at several widths $B2$ of the dogbone central part are shown in Fig. 7. Inspection of these plots shows that variation of $B2$ incurs simultaneous shift of both electric and magnetic resonances in the same direction, similarly to that in the case of variable $B1$, cf. Fig. 6. When the stripe width increases, the inductive response of the central stripes weakens (for both antisymmetric and symmetric modes), and both magnetic and electric resonances occur at higher frequencies. The qualitative interpretation of this phenomenon is further corroborated using the TL model of the dogbone particle in Section 4.

In contrast to $B2$ variations, the stripe width $A1$ of the dogbone lateral arms, at $A2$ kept unchanged, has distinctively different effect on the magnetic and electric resonances as illustrated in Fig. 8. Namely, when the lateral stripes become narrower, the f_m increases and f_e decreases. Therefore, they move in opposite directions and even can interchange their positions, i.e., the magnetic resonance may occur either below or above the electric resonance. Also, these resonances may degenerate as shown in Fig. 8 for $A1 = 0.5$ mm. It is necessary to note that width $A1$ has only marginal impact on f_e which slowly varies due to variations of the dogbone central part ($A2 - 2 \times A1$). Conversely, the magnetic resonance is strongly influenced by the width $A1$ when $A1$ becomes commensurable with thickness H of the dielectric spacer separating a pair of conductors in the dogbone particle of Fig. 2. Then, when the stripes become narrower, the capacitance between the top and bottom lateral arms of tightly coupled dogbones decreases and f_m rapidly moves towards higher frequencies. Thus the use of thin arms (small $A1$) is also a way to achieve the NRI effect when the dielectric spacer is present (see Section 5.2). Such

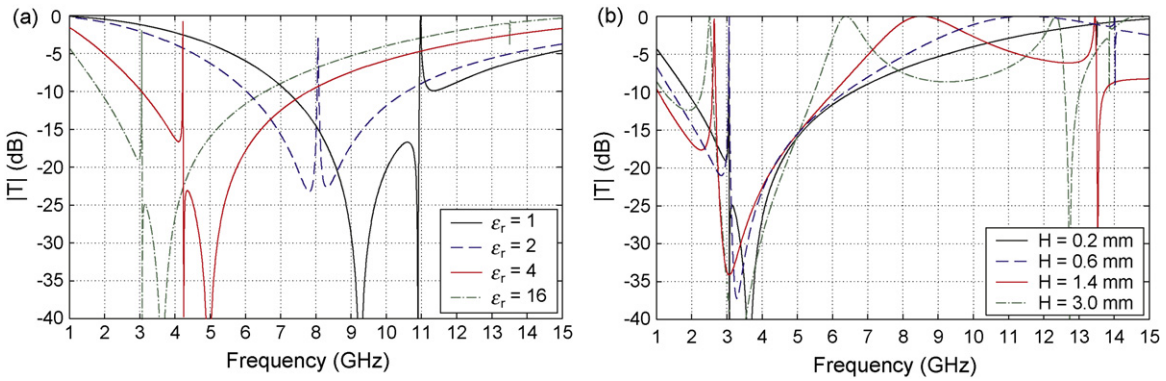

Fig. 9. Transmission coefficient for a doubly periodic planar array composed of the dogbone pairs shown in Fig. 2 vs. permittivity (ε_r) and thickness (H) of the dielectric spacer separating the top and bottom conductors in a dogbone pair. (a) Permittivity is variable (ε_r =1, 2, 4, 16) while thickness is fixed to $H = 0.2$ mm. (b) Thickness is variable ($H = 0.2$, 0.6, 1.4, 3) while permittivity is fixed to $\varepsilon_r = 16$: the electric and magnetic resonances occur at $f_e \approx 3.3$–3.7 GHz and $f_m \approx 2.5$–3.1 GHz, respectively.

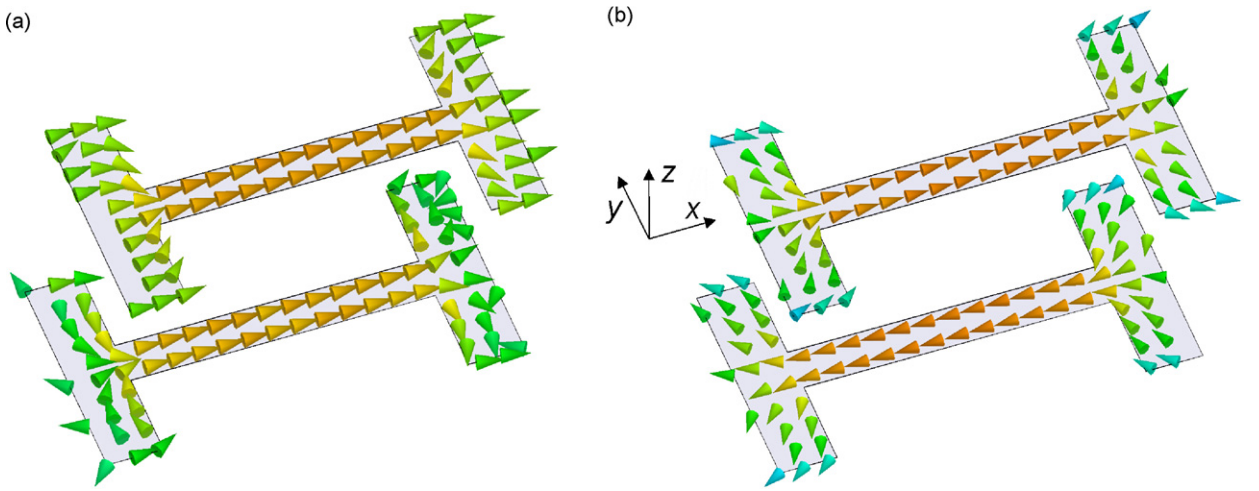

Fig. 11. Current distributions on a pair of tightly coupled dogbone conductors: (a) symmetric current distribution at $f = 9.1$ GHz near the frequency of electric resonance f_e; (b) antisymmetric current distribution at $f = 10.9$ GHz near the magnetic resonance frequency f_m. Note that in order to improve clarity of the plots, the spacing between the conductors is not to scale (in the simulations $H = 0.2$ mm).

behaviour of the magnetic resonance is also consistent with the predictions of the TL model discussed later in Section 4.

As mentioned in the preceding discussion, the magnetic resonance appeared to be particularly sensitive to the stripe width commensurate to the thickness H of the spacer separating the pairs of conductors in the dogbone particle in Fig. 2. Therefore, it is important to examine how the layer parameters affect the resonance frequencies, which are presented in Fig. 9. The transmission characteristics in Fig. 9(a) simulated for different values of the spacer permittivity ε_r reveal that variation of ε_r causes interchange of the magnetic and electric resonance positions with respect to each other. A similar feature was observed earlier in connection with the effect of $A1$ variations. However in contrast to the latter case, both types of resonances shift towards lower frequencies at higher ε_r, albeit f_e and f_m vary with substantially different rates. Indeed, the magnetic resonance should be more sensitive to ε_r because the fields are predominantly confined to the dielectric spacer between the dogbone conductors, cf. Section 3.2. The electric resonance is less affected because the electric field of the symmetric mode is mainly located outside the thin dielectric spacer.

Finally, the effect of separation H between the top and bottom dogbone conductors is demonstrated in Fig. 9(b). The magnetic resonance f_m barely varies with H, while H remains small. However at larger H, f_m decreases and the electric resonance undergoes considerable changes too. The latter phenomena cannot be described by the TL line model of a single particle presented in Section 4 since the fringing field effects at bends and stripe edges play a significant role at large ratios H/w, where w is the stripe width, either $A1$ or $B2$. Furthermore, when $H > (A - A2)$ the capacitive coupling between contiguous dogbone particles starts to affect significantly the magnetic resonance frequency.

With reference to the default dimensions of the dogbone particle, it is important to note that the lateral sizes of the unit cell ($A \times B$) at the magnetic resonance frequency $f_m \approx 3$ GHz equal $A = B = \lambda/13.3$, i.e., they are substantially smaller than the wavelength. This significant cell size miniaturization is due to the capacitance between the top and bottom parts of the dogbone particle, and to the permittivity of the dielectric spacer, both contributing to lower the magnetic resonance frequency. Therefore the induced magnetic dipole density is approximately equal to 176 effective magnetic dipoles per λ^2.

3.2. Dogbone pair of conductors in free-space

The mechanisms of the resonance formation in the dogbone particles (Fig. 2) are explored in this section in more detail. For the sake of simplicity, we assume the permittivity of the spacer between the conductors in the dogbone pair to be equal to $\varepsilon_r = 1$ while the structure dimensions (in mm) are held the same as in the preceding section: $A = 7.5$, $B = 7.5$, $B1 = 4$, $A2 = 7.4$, $B2 = 0.8$, $A1 = 1.0$, $H = 0.2$. Let us now examine the transmission coefficients $|T|$ shown in Fig. 10 for a doubly periodic planar array of dogbone pairs with isolated conductors and with short-circuited arms (see insert, Fig. 10).

Comparison of the plots for these two arrangements shows that in the frequency range shown in Fig. 10, only

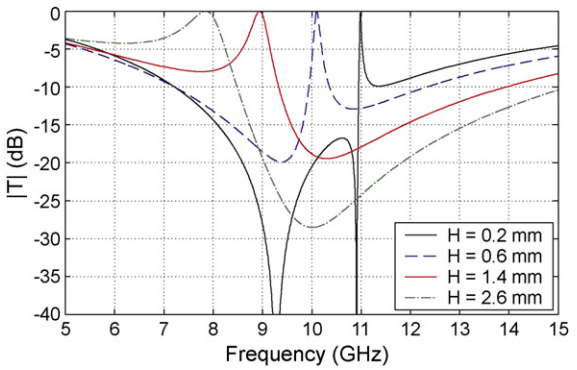

Fig. 12. Transmission coefficient $|T|$ at variable H in the doubly periodic planar arrays of dogbone pairconductors in *free-space*. The unit cell dimensions (in mm), $A = 7.5$, $B = 7.5$, $B1 = 4$, $A2 = 7.4$, $B2 = 0.8$, $A1 = 1.0$, are the same as in Fig. 3.

the resonance at $f_m \approx 10.9$ GHz is suppressed by short-circuiting the dogbone arms whilst the wide dip about frequency $f_e \approx 9.2$ GHz remains practically unaffected. The stopband response about f_e is typical of frequency selective surfaces, and the currents on the pair of dogbone conductors are in-phase (symmetric), as illustrated in Fig. 11(a). Therefore the pair of closely spaced short-circuited conductors essentially behaves like a single conductor, and no artificial magnetism is observed at f_e.

The narrow band resonance at frequency $f_m \approx 10.9$ GHz is associated with the antisymmetric current distributions in the pair of isolated dogbone conductors as demonstrated in Fig. 11(b). These oppositely directed currents form a magnetic dipole pointing at the y-direction and produce artificial magnetism near the frequency f_m. The properties of the antisymmetric modes in the dogbone pairs are comprehensively described by the TL model further elaborated in Section 4.

As already mentioned in the earlier discussion of Fig. 9, variations of the spacing permittivity between the dogbone conductors much stronger affect the magnetic resonance f_m than the electric resonance f_e. Comparison of Figs. 3 and 10 confirms this trend and suggests that such behaviour of f_m is related to a closer confinement of the antisymmetric TL mode to the interior of the dogbone particle. This implies that the capacitance between the top and bottom conductors in the dogbone pair strongly influences the magnetic resonance. To further examine this conjecture, let us consider how the conductor separation H affects f_m in the case of $\varepsilon_r = 1$. The simulation results in Fig. 12 show that while f_m decreases with increasing H, as was also observed in Fig. 9(b), the resonance curves significantly differ here. Namely, at small values of $H \sim 0.2$–0.6 mm, $f_m > f_e$, and the magnetic resonance is readily identifiable. But when H increases further to 1.4–2.6 mm, not only becomes $f_m < f_e$ but also the Q-factor considerably decreases. The latter qualitative changes in the magnetic resonance behaviour cannot be explained within a single mode TL model because the capacitive coupling between the top and bottom conductors in a pair may become weaker than that between the pairs in the adjacent cells. In these circumstances, interaction between contiguous dogbone particles affects also the magnetic resonance as the distance between the contiguous conductors $(A - A2) = 0.1$ mm becomes considerably smaller than the separation H between the top and bottom conductors in the pair (in this geometry $A = 7.5$ mm and $A2 = 7.4$ mm). Moreover, at larger H, the fringing field effects are more significant as the conductor separation ($H = 1.4$ mm) exceeds the stripe widths $A1 = 1$ mm or $B2 = 0.8$ mm.

For the free-space arrangement, the particle size at the magnetic resonance frequency of $f_m \approx 10.9$ GHz is as small as $A = B = \lambda/3.67$. Though in the absence of a dielectric spacer the size reduction, with respect to the wavelength, is less than that in Section 3.1, considerable miniaturisation has been achieved, owing to the strong capacitive coupling between the top and bottom parts of the dogbone particle.

The presented analysis has demonstrated that the dogbone particles provide a means for controlling the positions of the electric and magnetic resonances. This property is of particular importance for the implementation of an artificial medium with NRI. In Section 5 we will show that dogbone pairs can be used to realize a medium supporting backward wave propagation at frequencies near f_m. If homogenization is allowed, backward wave propagation occurs when both the effective permittivity and permeability are negative. This double-negative requirement is generally satisfied near f_m, as long as $f_m > f_e$, because the magnetic resonance is usually much narrower than the electric one[1]. To fulfill the condition $f_m > f_e$, it is necessary either to increase f_m or to decrease f_e. The f_e can be reduced either by increasing the capacitance between the contiguous dogbones or by making the dogbone longer, cf. Figs. 3 and 5. Alternatively f_m can be increased in the dogbone with narrower lateral arms (Fig. 8), or with thinner or lower permittivity dielectric spacers between the top and bottom conductors in the dogbone particle (Figs. 9 and 12).

[1] As shown in Fig. 14, the magnetic resonance becomes broader at larger H. In this case the condition $f_m > f_e$ may not be strictly required for realizing NRI.

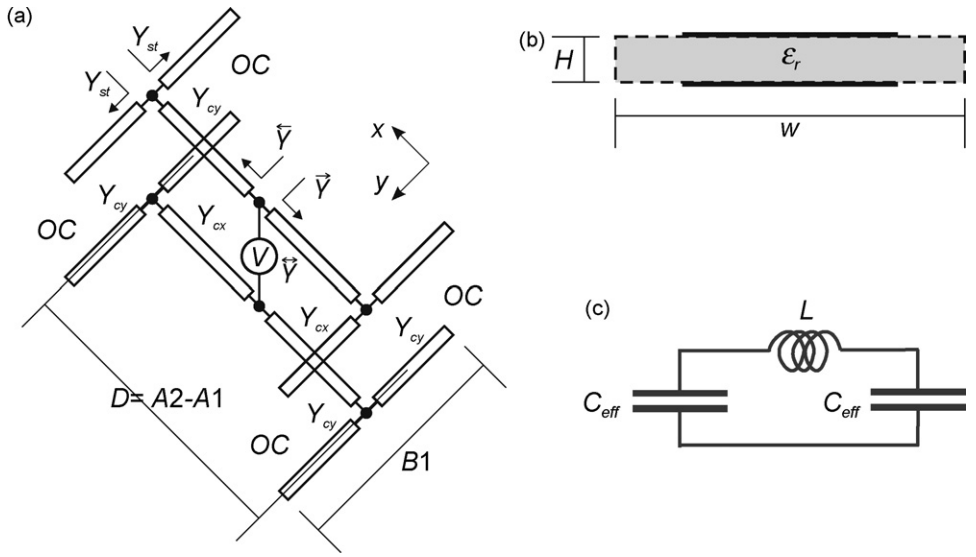

Fig. 13. (a) TL model for antisymmetric distribution of currents on a single dogbone particle. (b) Cross-section of the TL. The stripes have separation H and width $w = B2$ or $w = A1$. They are be separated by a dielectric slab with dielectric constant ε_r. (c) Simplified LC resonant circuit approximating the magnetic resonance for a dogbone particle.

In order to gain a deeper insight in the effects of the geometrical parameters on the fundamental properties of the dogbone particles, a TL model of the dogbone pairs has been developed and will be discussed in the next section.

4. Approximate transmission line model for magnetic resonances

In the antisymmetric mode, an isolated dogbone conductor pair (we neglect coupling between adjacent cells) can be approximately described by an equivalent circuit composed of interconnected sections of TLs. Namely, the dogbone "arms" are represented as open-circuit (OC) stubs with characteristic admittance Y_{cy} and wavenumber β_y of the quasi-TEM (transverse electric and magnetic) or pure TEM (at $\varepsilon_r = 1$) wave propagating along the y-axis (see Figs. 2 and 13) with the time dependence $\exp(j\omega t)$. These stubs provide the shunt admittances $Y_{st} = jY_{cy}\tan(B1\cdot\beta_y/2)$ at the reference ports where they are connected to the TL central section of length $D = (A2 - A1)$ along the x-direction which has the characteristic admittance Y_{cx} and wavenumber β_x, see Fig. 13. The length D is defined as the distance between the two mid-points in the dogbone "arms".

To evaluate the characteristic admittances Y_c and wavenumbers β of the TLs and stubs, it is convenient to express them in terms of the capacitance C_l and the inductance L_l per unit length (subscripts x, y are temporary omitted here because the same expressions are used for both the TL central section and stubs):

$$Y_c = \sqrt{\frac{C_l}{L_l}}; \qquad \beta = \omega\sqrt{C_l L_l} = \frac{\omega}{v_p} \tag{1}$$

where ω is the angular frequency and $v_p = 1/\sqrt{C_l L_l}$ is the phase velocity of the propagating wave.

C_l and L_l for the TL with the cross-section shown in Fig. 13(b) can be evaluated by using the standard approximations for microstrip lines with quasi-TEM waves [35]. For the quasi-TEM wave, v_p is alternatively defined as $v_p = c/\sqrt{\varepsilon_r^{eff}}$ where $c = 1/\sqrt{\varepsilon_0\mu_0}$ is the speed of light in free-space, ε_0 and μ_0 are the permittivity and permeability of free-space, and ε_r^{eff} is a relative *effective* permittivity of the equivalent homogeneous medium filling the TL cross-section, which may differ for a TL along the x- and y-direction. For a quasi-TEM mode on the TL shown in Fig. 13(b), ε_r^{eff} can be approximated as follows [35]:

$$\varepsilon_r^{eff} \approx \frac{\varepsilon_r + 1}{2} + \frac{\varepsilon_r - 1}{2}\frac{1}{\sqrt{1 + 6/r}} \tag{2}$$

where $r = w/H$ is the TL aspect ratio; w is the width of stripes: either $B2$ (for a TL along x) or $A1$ (for a TL along y) and H is the separation between them, Fig. 13(b). Making use of the effective permittivity ε_r^{eff}, the capacitance per unit length C_l is represented as follows:

$$C_l \approx \varepsilon_r^{eff}\varepsilon_0\overline{C} \quad [\mathrm{F/m}] \tag{3}$$

where $\bar{C}$ is the capacitance per unit length of the pair of stripes in free-space, normalized to ε_0. Several approximations are available to calculate $\bar{C}$, see [35,36], and the following closed form expressions with relative error less than $\pm 1\%$ at any aspect ratio r is used here:

$$\bar{C} \approx \begin{cases} r + 1.21 - \dfrac{0.11}{r} + \dfrac{1}{2}\left(1 - \dfrac{1}{2r}\right)^6, & 2r \geq 1 \\ \dfrac{\pi}{\ln((4/r)+(r/2))}, & 2r \leq 1. \end{cases} \tag{4}$$

The inductance per unit length L_l is readily expressed in terms of $\bar{C}$ with the aid of (1) and (3):

$$L_l = \frac{1}{v_p^2 C_l} = \frac{\mu_0}{\bar{C}}. \tag{5}$$

Then the characteristic admittance Y_c takes the form:

$$Y_c = \sqrt{\frac{C_l}{L_l}} \approx \frac{\sqrt{\varepsilon_r^{eff}}}{\eta_0}\ \bar{C}. \tag{6}$$

where $\eta_0 = \sqrt{\mu_0/\varepsilon_0} = 120\pi\ \Omega$ is the free-space impedance and the parameters ε_r^{eff}, $\bar{C}$ are given by (2) and (4).

In the case when the whole transmission line is filled with a homogeneous medium (for example, air) with permittivity ε_r, one shall have $\varepsilon_r^{eff} = \varepsilon_r$, $v_p = c/\sqrt{\varepsilon_r}$, $\beta = k_0\sqrt{\varepsilon_r}$, and $Y_c \approx \sqrt{\varepsilon_r}\ \bar{C}/\eta_0$. These expressions are applicable to the TL segments along both the x- and y-directions. If all TLs are identical or $\varepsilon_r = 1$ (free-space) $\beta_x = \beta_y$, whereas the characteristic admittances Y_{cx}, Y_{cy} are equal only if the TLs are identical along both axes. In the case of free-space, $\beta_x = \beta_y = \omega\sqrt{\mu_0\varepsilon_0} = \omega/c$.

The resonance frequency f_m for the TL circuit shown in Fig. 13 is obtained by evaluating the total input admittance $\overleftrightarrow{Y} = \overleftarrow{Y} + \overrightarrow{Y}$ at a reference port of the equivalent circuit, where $\overleftarrow{Y}$ and $\overrightarrow{Y}$ are the admittances of the TL looking toward opposite directions from this port. The resonances of the dogbone particle occur at frequencies that render either $\overleftrightarrow{Y} = \infty$ or $\overleftrightarrow{Y} = 0$. When the admittance $\overleftrightarrow{Y}$ is evaluated at the central part of the dogbone, the symmetry conditions apply ($\overleftarrow{Y} = \overrightarrow{Y}$). Here we are interested in the lowest resonance f_m, whose mode has a maximum current at the center of the dogbone that maximizes the strength of the magnetic dipole moment. Therefore, at this resonance it is necessary that $\overleftrightarrow{Y} = \infty$, viz:

$$\overleftarrow{Y} = \overrightarrow{Y} = Y_{cx}\frac{2Y_{st} + Y_{cx}\,s}{Y_{cx} + 2Y_{st}\,s} = \infty \tag{7}$$

where $s = j\tan(\beta_x D/2)$, $Y_{st} = jY_{cy}\tan(B1\cdot\beta_y/2)$ and Y_{cx}, Y_{cy} are calculated with the aid of (6). Here we have assumed that the dogbone particle may comprise the TL sections of dissimilar shapes along the x- an y-axes that results in different characteristic admittances Y_{cx}, and Y_{cy} and wavenumbers β_x and β_y given by (1).

The condition $\overleftrightarrow{Y} = \infty$ requires the denominator of (7) to vanish, i.e., the resonance occurs at

$$Y_{cx} + 2Y_{st}\,s = 0. \tag{8}$$

The solutions of (8) can be obtained numerically or approximately as detailed below. Note that in this model we have neglected fringing capacitances of the TL in open circuit stubs, and reactances at the TL bends and junctions. In most cases such approximations are found to be satisfactory and give adequate qualitative and approximate quantitative results. Alternatively, corrections can be introduced by means of effective elongation of the respective TL sections.

4.1. Approximate resonance condition

The above equations are simplified here to determine approximate values of f_m. In the case of $\beta_x D/2 \ll \pi/2$ and $B1\cdot\beta_y/2 \ll \pi/2$, with $D = A2 - A1$, we can use the following approximations: $s \approx j\beta_x D/2$ and $Y_{st} = jY_{cy}B1\cdot\beta_y/2$. Accordingly, the resonance condition (8) takes the form

$$Y_{cx} - Y_{cy}\cdot\beta_y\cdot\beta_x\cdot B1\cdot D/2 = 0, \tag{9}$$

which gives the magnetic resonance angular frequency

$$\omega_m = \sqrt{v_{p,x}v_{p,y}}\sqrt{\frac{Y_{cx}}{Y_{cy}}}\sqrt{\frac{2}{B1\cdot D}} = \frac{c}{\sqrt{\varepsilon_{r,y}^{eff}}}\sqrt{\frac{\bar{C}_x}{\bar{C}_y}}\sqrt{\frac{2}{B1\cdot D}}. \tag{10}$$

It is interesting to note that the same result can be obtained from the electrostatic and magnetostatic approximations for the capacitance and inductance of the dogbone. The total capacitance of the dogbone is associated with the charge accumulated on its lateral arms, each of which approximately contributes

$$C_{eff} = \varepsilon_0\varepsilon_{r,y}^{eff}\frac{A1\ B1}{H}, \tag{11}$$

where we have neglected the fringing effects (this is a satisfactory approximation for $w \gg H$). A similar approximation for the total inductance of the central section of the dogbone, where the current is maximal, is given by

$$L_{eff} = \mu_0\frac{H}{B2}D. \tag{12}$$

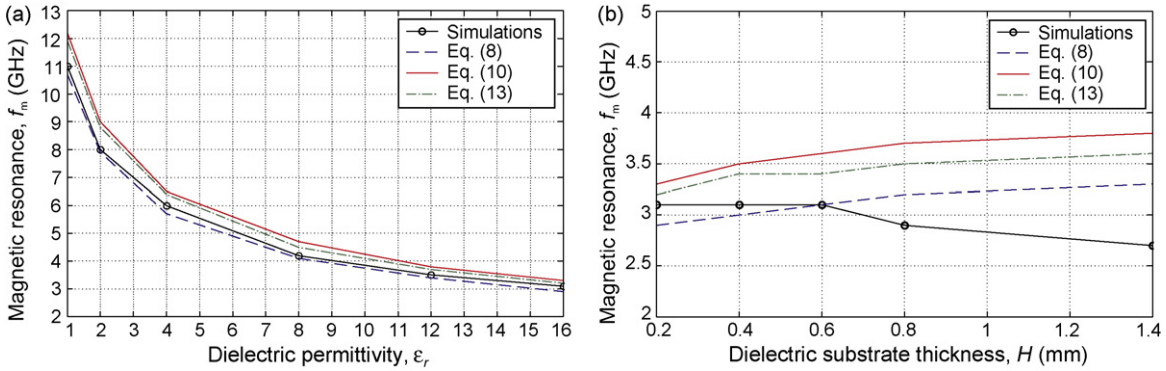

Fig. 14. Magnetic resonance frequency f_m vs. permittivity (ε_r) and thickness (H) of the dielectric spacer supporting the dogbone particle. Data obtained from the rigorous numerical simulations (assuming a periodic structure) are compared with the approximate formulas (8), (10) and (13) based on the TL model of the dogbone particle. (a) Permittivity is variable while thickness $H = 0.2$ mm is fixed. (b) Thickness H varies while permittivity $\varepsilon_r = 16$ is fixed.

Then, taking into account the capacitive contributions of both dogbone arms (cf. Fig. 13(c)), the magnetic resonance ω_m equals

$$\omega_m = \frac{1}{\sqrt{L_{eff} C_{eff}/2}} = \frac{c}{\sqrt{\varepsilon_{r,y}^{eff}}} \frac{\sqrt{2 \cdot B2}}{\sqrt{B1 \cdot A1 \cdot D}} \qquad (13)$$

which is identical to (10) when the characteristic impedances are equal $Y_{cx} = Y_{cy}$ (and thus $B2 = A1$) and $v_{p,x} = v_{p,y}$.

4.2. Accuracy and limitations of the TL model

In this section we assess the relative accuracy and applicability of the TL approximations developed here to evaluate f_m of the dogbone particle. The results presented in Fig. 14 summarize the magnetic resonance dependence on the parameters of the dielectric spacer, namely, its permittivity ε_r and thickness H, to which f_m was found particularly sensitive in the preceding parametric study, cf. Figs. 9 and 12.

In Fig. 14(a), f_m was calculated at several values of permittivity ε_r, while the dogbone geometrical parameters assumed the default values (in mm): $A = B = 7.5$, $C = 8$, $B1 = 4$, $A2 = 7.4$, $B2 = 0.8$, $A1 = 1$, $H = 0.2$. The reference data for f_m (black curve) have been retrieved from the transmission response of a doubly periodic array of dogbone particles simulated numerically at $\varepsilon_r = 1$, 2, 4, 8, 12, 16 as described in Section 3. The other curves represent the f_m estimates obtained from Eqs. (8), (10), and (13). It appears that for the considered configuration with a small separation between the top and bottom conductors in the dogbone particle, all the approximations based on a TL model provide an accurate prediction of the magnetic resonance frequency. Furthermore, they exhibit the same trend observed earlier in Fig. 9 that f_m rapidly decreases with ε_r, thus reconfirming the fact that the fields of the antisymmetric mode are tightly confined to the dielectric spacer separating the pair of dogbone conductors.

The TL approximations have also been assessed in Fig. 14(b) for a variable thickness H of the dielectric spacer with permittivity $\varepsilon_r = 16$ between the top and bottom conductors of the dogbone pair. The f_m values deduced from the rigorous numerical simulations of a doubly periodic array of dogbone particles are compared again with the corresponding approximate values obtained from Eqs. (8), (10), and (13). The plots in Fig. 14(b) show that f_m stays practically constant at small values of H, and the f_m approximations are in reasonable agreement with the results of numerical simulations. However, when H grows, the numerical simulations show an appreciable decrease of f_m, as was also observed in Figs. 9(b) and 12. However, the TL formulas no longer provide a satisfactory approximation for f_m at larger H. This indeed is not surprising since these approximate formulas completely neglect the fringing capacitances at the TL ends and bends, and the capacitive coupling between the adjacent cells, which become even more pronounced at larger H. The latter interaction affects not only the electric but also the magnetic resonance when the separation H between the top and bottom conductors in the pair exceeds the distance $(A - A1)/2$ between the contiguous particles. Therefore, the rapid variation of f_m at large values of H cannot be described by a simple TL model for a *single isolated* particle, and the collective response of the array will be modeled more accurately in a future investigation.

The results presented in Fig. 14 allow one to conclude that in spite of their limitation, the developed analytical

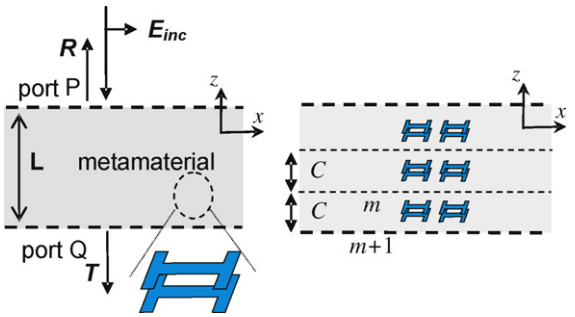

Fig. 15. Metamaterial composed of stacked layers of the arrayed dogbone particles (Fig. 2). In order to identify the existence of backward wave propagation, phase variations of the waves transmitted through the stack are analyzed at the reference ports P and Q when increasing the number of stacked layers.

models provide an adequate qualitative description for a broad range of dogbone configurations. These approximations give an insight into the effect of the structure parameters on the magnetic resonance and are instrumental in the initial design of the constituent dogbone particles for the specified frequency response.

5. Backward wave propagation in a medium formed by stacked layers of dogbone particles

In this section we show that metamaterials composed of stacked layers of dogbone particles comprised of tightly coupled pairs of conductors as shown in Fig. 2, can support backward wave propagation in certain frequency bands. To illustrate this phenomenon, we adopt two methods based on numerical simulations. The first approach is rather qualitative and may be affected by the interface effects, while the second one is based on the rigorous analysis of the Brillouin dispersion diagram for an infinite stack of dogbone layers periodic along the z-direction.

In the first method, the magnitude and phase progression/regression in the transmitted waves is evaluated by varying the numbers of stacked layers. The phase variation of the scattering parameter S_{QP} (S_{21} in the standard terms) between the reference interfaces P and Q (Fig. 15) equals

$$\Delta\varphi = \varphi_Q - \varphi_P \approx -k_M L \tag{14}$$

where k_M is the wavenumber in the metamaterial and L is the stack thickness. For the time convention $\exp(j\omega t)$ used, $\Delta\varphi < 0$ corresponds to forward wave propagating with $k_M > 0$, whereas $\Delta\varphi > 0$ and $k_M < 0$ are associated to backward wave propagation. This approach gives accurate results when reflection at the air/material interfaces is negligible in the analyzed frequency band.

A simple approximate procedure similar to that used in Ref. [16] is applied first to determine the k_M sign. Namely, we increase the number m of the stacked layers of dogbone pairs spaced apart in z-direction for distance C, which corresponds to the unit cell height in Fig. 2 or equivalent "layer" thickness. Then for the total stack thickness $L = mC$, where $m = 1, 2, \ldots$, we evaluate the phase difference $\Delta\varphi$ at the interfaces Q and P. To make the method less dependent of the interface properties, we analyze the incremental phase difference $\Delta\varphi_m^{m+1}$ between the cases of m and $(m+1)$ layer stacks. In particular, for backward wave propagation in a multilayered metamaterial, the phase φ_{m+1} at the $(m+1)$th layer interface is larger than the phase φ_m at the mth layer interface that gives

$$\Delta\varphi_m^{m+1} = \varphi_{m+1} - \varphi_m = -k_M C > 0. \tag{15}$$

A number of recent studies are concerned with the homogenization of the artificial medium, though this topic is still extensively debated in the context of metamaterials. Homogenization aspects of the dogbone-based layered medium are beyond the scope of this paper, therefore we will not discuss the frequency ranges where this is permitted. Nevertheless, the relevant basic concepts will be used here with the sole purpose of providing the coherent definitions of the characteristics adopted in our approach. We will not retrieve the effective medium permeability and permittivity parameters, but we will obtain an approximation for an *effective* refractive index n. Accordingly, for a wave traveling along the z-direction with electric field polarized along the x-direction, the wavenumber can be defined as $k_M = nk_0$, where k_0 is the free-space wavenumber. Therefore in this paper, n is used only as a derived parameter strictly related to the phase velocity of a wave with fixed polarization and incidence angle. Then we can retrieve n by using the method employed in Ref. [16] for SRR metamaterials and determine n from the incremental phase difference as follows:

$$n \approx -\frac{\Delta\varphi_m^{m+1}}{k_0 C}. \tag{16}$$

The second method adopted here is based upon a rigorous analysis of wave propagation in infinite periodic lattices. We evaluate numerically the dispersion characteristics (frequency vs. wavenumber k_M along z) for the doubly periodic (in x–y plane) planar arrays of dogbone pairs stacked along the z-direction with period C (Fig. 15). The dispersion diagrams are obtained by the eigenmode solver in CST Microwave Studio with periodic boundary conditions applied to the unit cell with the dogbone conductor pair shown in Fig. 2. The simulated

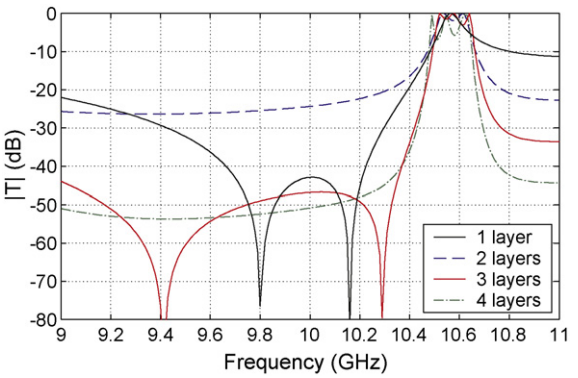

Fig. 16. Transmission coefficient for a few layers of arrayed dogbone particles stacked along the z-direction with period $C = 2.6$ mm (similar results for a single layer of dogbone particles are shown in Fig. 12 with the only difference that here $H = 0.4$ mm and several layers are included). The electric resonance f_e is in the band 9.4–9.8 GHz, the magnetic resonance f_m is in the band 10.5–10.65 GHz.

structure is periodic along the x-, y- and z-directions, with the lattice constants A, B, and C, respectively. The examples below illustrate applications of the two aforementioned approaches.

5.1. Example: dogbone pairs in free-space

Let us consider a slab composed of several stacked layers of arrayed dogbone particles in free-space (i.e., the permittivity of a spacer between the paired conductors in the dogbone particle is $\varepsilon_r = 1$). The geometric parameters (in mm) are the same as in Section 3.1: $A = 7.5$, $B = 7.5$, $B1 = 4$, $A2 = 7.4$, $B2 = 0.8$, $A1 = 1.0$, and the interlayer period is $C = 2.6$ mm. The separation between the paired conductors in the dogbone particle is chosen $H = 0.4$ mm to realize $f_m > f_e$ (according to the data in Fig. 12, the latter inequality is held at any $H \leq 0.6$ mm). The simulation results in Fig. 16 show that a transmission peak exists between 10.5 and 10.65 GHz, which is associated with the artificial magnetism at the magnetic resonance, as already discussed in Section 3.2 (cf. current distribution in the antisymmetric mode shown in Fig. 11 for $H = 0.2$ mm).

The transmission coefficient T magnitude and phase for this structure is zoomed in Fig. 17 around the transmission peaks corresponding to the magnetic resonance. From the phase plots in Fig. 17(b), we can readily infer that the phase $\Delta\varphi$ of the transmission coefficient T increases with the number of layers, thus showing that a phase difference $\Delta\varphi_m^{m+1} > 0$ can be realized. Hence the structure supports *backward wave* propagation along the z-direction in the frequency band $10.5 - 10.65$ GHz.

According to Eq. (16), the refractive index n for the case shown in Fig. 17 varies with frequency in the range $n \approx -2$ to -3.5. The results are not completely stable when the number of layers is increased because of the interlayer couplings and reflections at the two air-metamaterial interfaces. Nevertheless, the qualitative trend of the n behaviour remains consistent when the number of stacked layers increases.

An alternative proof of the existence of backward wave propagation has been obtained from the dispersion characteristics for the infinite periodic (along the z-direction with period $C = 2.6$ mm) arrangement of stacked layers of the arrayed free-space dogbone particles with the same parameters as in Figs. 16 and 17. The one-dimensional dispersion diagrams for the spacing $H = 0.2$, 0.4, 0.6 mm between the top and bottom conductors in the dogbone particle are presented in Fig. 18. The three branches shown in Fig. 18(a) correspond to the low-frequency region of the dispersion diagram of the dogbone particle lattice. The lower and upper frequency branches correspond to the usual low-frequency passband that is split in two portions by the resonant stop-

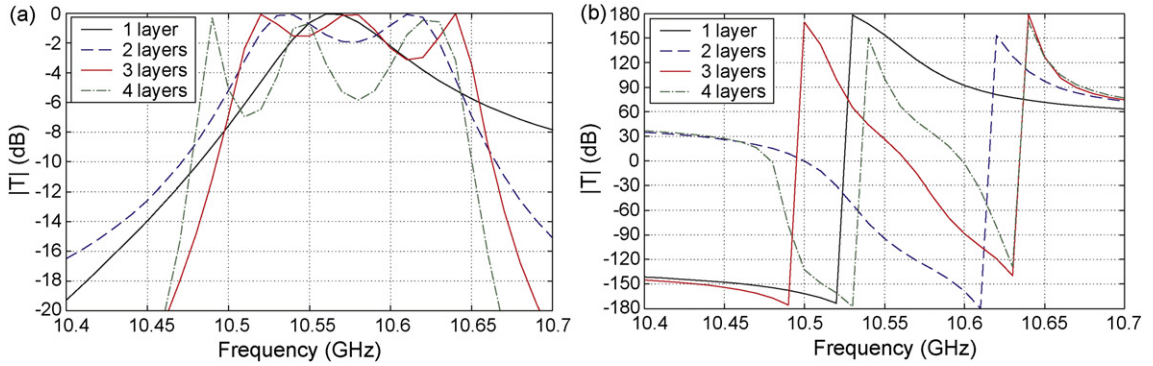

Fig. 17. Magnitude (a) and phase (b) of the transmission coefficient for a few layers of arrayed dogbone particles, stacked along the z-direction with the interlayer period $C = 2.6$ mm. Within the passband at 10.5–10.65 GHz occurring in the vicinity of the magnetic resonance, backward wave propagation exists because of the phase difference $\Delta\varphi_m^{m+1} > 0$.

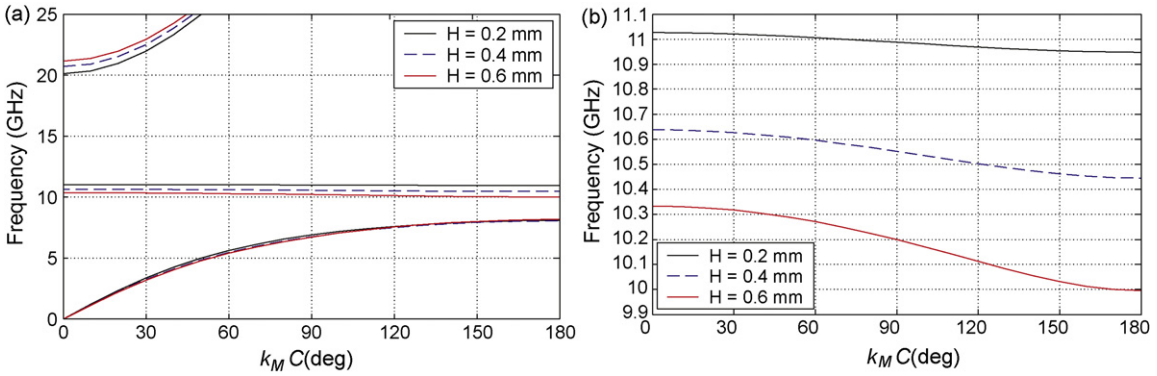

Fig. 18. Dispersion diagrams for an infinite periodic (along the z-direction with period $C = 2.6$ mm) arrangement of stacked layers of the arrayed free-space dogbone particles with spacer thicknesses $H = 0.2$, 0.4, 0.6 mm. The structure parameters are the same as in Fig. 17. (a) Low-frequency dispersion diagram of the dogbone particle lattice. (b) Enlargement of the NRI passband (the negative slopes indicate backward wave propagation). If the lateral arms of the pair of dogbones would be short-circuited (cf. Figs. 3 and 10), or, in an analogous manner, the dogbone pairs in each cell would be replaced by a single dogbone conductor, the second passband with negative slop would disappear.

band occurring far below the Bragg resonance due to a lattice of resonant electric scatterers. A narrow passband in the middle arises as the result of the superposition of the electric and magnetic resonances of the dogbone particles. We have numerically verified that it disappears when the lateral arms of the dogbone pair are short-circuited (see also Figs. 3 and 10) or the dogbone particle contains only a single dogbone-shaped conductor. Thus, the middle branches of the dispersion diagram, which are shown in more detail in Fig. 18(b), exist only in the presence of both the magnetic and electric resonances of the dogbone particles and represent backward waves with oppositely directed phase and group velocities. In this frequency band the lattice of dogbone particles can be homogenized and characterized as a NRI medium.

The backward wave propagation for all three thicknesses of spacing between the dogbone pair conductors is confirmed by the negative slope of the dispersion curves in Fig. 18(b). These plots also show that for small values of H the NRI passband is narrow, as already demonstrated in Figs. 16 and 17, but a broader NRI band can be achieved at larger H, which provides a better overlap of the electric and magnetic resonances. These results are in full agreement with what we have observed in Fig. 12, and also show that the f_m decreases at larger H.

5.2. *Example: dogbone pairs with low permittivity dielectric spacers*

In this example, we consider stacked layers of the arrayed dogbone particles printed on the opposite faces of a dielectric substrate (spacer) with permittivity $\varepsilon_r = 2.2$. The structure dimensions (in mm) are $A = B = 7.5$, $B1 = 4$, $A2 = 7.4$, $A1 = B2 = 0.5$.

The simulated magnitude of the transmission coefficient $|T|$ through a single layer of the planar array of dogbone particles is shown in Fig. 19, for several thicknesses H of the dielectric substrate separating the top and bottom conductors. A narrow passband, which corresponds to the magnetic resonance of the dogbone pair and strongly depends on H, is readily observable in the plots.

The dispersion diagrams for an infinite periodic (along the z-direction with the period $C = 3$ mm) arrangement of stacked layers of the arrayed dogbone particles printed on the opposite faces of a dielectric substrate with $\varepsilon_r = 2.2$ and thicknesses $H = 0.25$, 0.5, 1 mm are presented in Fig. 20 (the other dimensions of the structure are the same as in Fig. 19). While the fun-

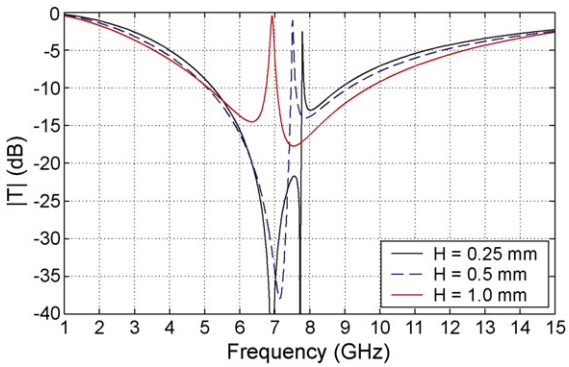

Fig. 19. Transmission coefficient $|T|$ for a single layer of arrayed dogbone particles made of a pair of conductors printed on a low permittivity dielectric substrates ($\varepsilon_r = 2.2$) of several thicknesses: $H = 0.25$, 0.5, 1 mm. The structure dimensions (in mm) are: $A = B = 7.5$, $B1 = 4$, $A2 = 7.4$, $A1 = B2 = 0.5$.

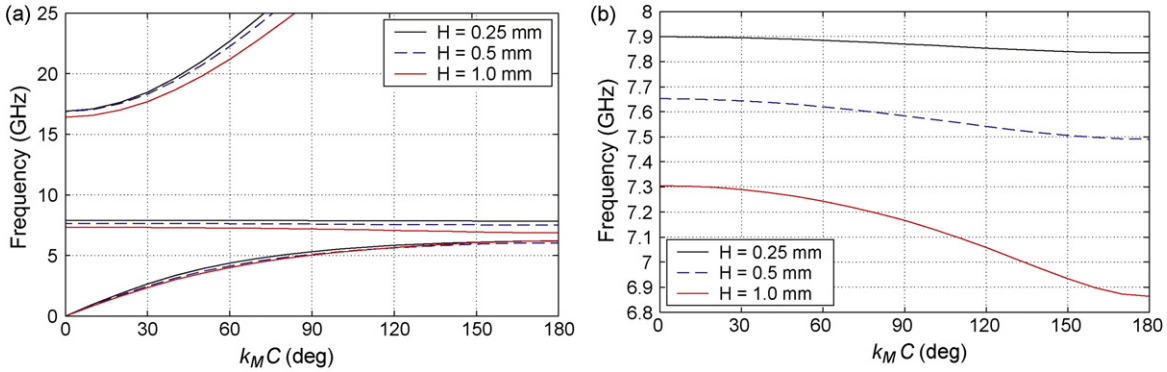

Fig. 20. Dispersion diagrams for an infinite periodic (along the z-direction with period $C = 3$ mm) arrangement of stacked layers of the arrayed dogbone particles printed on the opposite faces of dielectric substrates with permittivity $\varepsilon_r = 2.2$ and thicknesses $H = 0.25$, 0.5, 1 mm. (a) Low-frequency dispersion diagram of the dogbone particle lattice. (b) Enlargement of the double-resonant passband (the negative slopes indicate backward wave propagation).

damental properties of a NRI medium discussed in the preceding example for the free-space arrangement still hold in this case, the presence of the dielectric substrate adds new features. This is particularly concerned with the width of the NRI passband. Indeed, inspection of Figs. 18(b) and 20(b) shows that the NRI fractional bandwidth (Df/f_m, where Df is the absolute bandwidth) increases in the case of the dielectric substrate, and Df is broader for thicker substrates. Moreover, comparison of the dispersion curves for $H = 1$ mm in Figs. 18(b) and 20(b) shows that the Df becomes broader in the latter case as well. These results indicate that the use of the high permittivity dielectric substrates can lead not only to miniaturisation of the dogbone particles but also to a broader bandwidth of the NRI performance of such an artificial medium.

It is important to note that in the NRI frequency bands shown in Fig. 20(b), the ratio of the wavelength to the lattice constant A is of an order $\lambda/A \approx 6$. Therefore the low-frequency NRI bands are not related to the higher order Brillouin zones of the photonic crystals where the condition $A \ll \lambda$ is not satisfied.

The above dispersion analyses have been repeated in Fig. 21 when $B1 = B2 = 0.5$ mm and the dogbones conductors are reduced to simple short strips (*cut-wires*). All other parameters are as in Fig. 19, i.e., $A = B = 7.5$ mm, $A2 = 7.4$ mm, and the particles are printed on the opposite faces of dielectric substrates with $\varepsilon_r = 2.2$ and thicknesses $H = 0.25$, 0.5, 1 mm. It is found that although also a strip-pair medium can provide backward waves, the NRI transmission band for this structure occurs at significantly higher frequencies, which limits its applicability as a NRI medium. It is important to note that in the NRI frequency bands shown in Fig. 21(b), the ratio of the wavelength to the lattice constant A is of an order $\lambda/A \approx 3.5$.

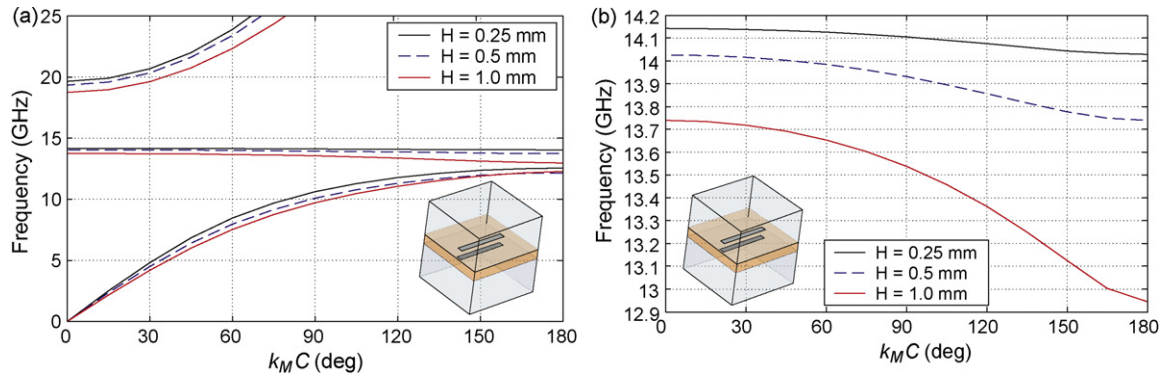

Fig. 21. Dispersion diagrams for an infinite periodic (along the z-direction with period $C = 3$ mm) arrangement of stacked layers of arrayed strip pairs (degenerated dogbone particles with $B1 = B2 = 0.5$ mm and other dimensions as in Fig. 19). The strips are located on the opposite faces of dielectric substrates with permittivity $\varepsilon_r = 2.2$ and thicknesses $H = 0.25$, 0.5, 1 mm as in Fig. 20. (a) Low-frequency dispersion diagram of the paired strip lattice. (b) Enlargement of the NRI passband.

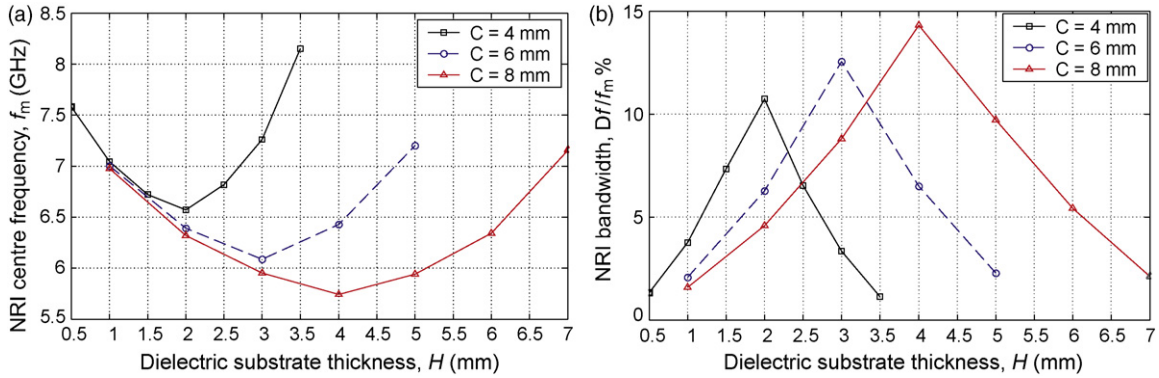

Fig. 22. Central frequency f_m (a) and fractional bandwidth Df/f_m (b) of the backward wave passband vs. thickness H of the dielectric substrate supporting the dogbone pairs in the infinite periodic (along the z-direction with period C) arrangements of the stacked planar arrays of dogbone particles. The structure dimensions and layout are the same as in Fig. 19.

To assess the concurrent effect of the dielectric spacer thickness H and the lattice constant C (along the propagation direction) on the NRI centre frequency f_m and fractional bandwidth Df/f_m these characteristics have been retrieved from the preceding dispersion analysis and are shown in Fig. 22. The analyzed dogbone structure is the same as that in Fig. 19, except that now H and C are variable. As apparent from Fig. 22(a), f_m progressively moves towards lower frequencies at larger H until it reaches its minimum at $H \cong C/2$, and then it starts to grow. Furthermore, the plots in Fig. 22(b) demonstrate that at the f_m minimum the NRI bandwidth Df/f_m reaches its maximum and can exceed 10%. Thus we can conclude that arrays of dogbone pairs with a proper aspect ratio can provide a reasonable bandwidth of NRI performance at low frequencies. Combined with the truly sub-wavelength size of the dogbone particles, the presented structures offer new opportunities for the practical realization of a homogenized NRI medium.

6. Conclusions

The properties of a recently proposed metamaterial arrangement based upon periodic arrays of tightly coupled pairs of dogbone shaped planar conductors have been explored in detail. A comprehensive parametric analysis was carried out to evaluate the impact of individual characteristic dimensions of the constituent unit cell and the dogbone particle onto the electromagnetic response of the metamaterial. It has been shown that this structure supports backward wave propagation in a rather broad band of the low-frequency region. We have conclusively demonstrated that these properties are associated with the electric (symmetric) and magnetic (antisymmetric) resonances of the tightly coupled conductor pairs, and the effective negative refractive index can be achieved, when the frequency of magnetic resonance is above the electric resonance. The origins of the artificial magnetism in the dogbone particles were explored, and it was shown that a magnetic dipole is created by a current loop on the pair of tightly coupled conductors with the antisymmetric current distribution.

We have developed an approximate model of the constitutive dogbone particles, based on a transmission line analysis. The model provides an accurate prediction of the magnetic resonance frequency and gives physical insight into the mechanisms of the resonance formation. The conditions of the magnetic resonance existence were obtained and the effect of the dogbone parameters on the resonance frequency was assessed. It has been shown that the lateral arms in the dogbone particles play a crucial role in controlling both the electric and magnetic resonances. The model suggested a means for controlling the magnetic resonance frequency and enabled an efficient design of the dogbone particles with the specified properties.

It has been demonstrated that backward wave propagation along the z-direction is supported in a metamaterial made of the stacked layers of the arrayed dogbone particles. This feature has been confirmed by monitoring the phase variation of a plane wave at the output interface of the layers' stack, when increasing the number of layers. The existence of backward wave propagation has also been inferred from the dispersion diagrams for the infinite periodic arrangement of the stacked layers of the arrayed dogbone particles. Comparison with a metamaterial made of layers of paired cut-wires has demonstrated that the dogbone shaped conductor pairs provide better control of the NRI band position.

The studied metamaterial has the advantage that it can be fabricated and assembled in planar technology. The

closely spaced pairs of dogbone shaped planar conductors naturally couple to the magnetic field of normally incident plane waves and readily exhibit the magnetic resonance of the antisymmetric mode.

References

[1] J.B. Pendry, A.J. Holden, D.J. Robbins, W.J. Stewart, Magnetism from conductors and enhanced nonlinear phenomena, IEEE Microwave Theory Technol. 47 (1999) 2075–2084.

[2] R. Marques, J. Martel, F. Mesa, F. Medina, Left-handed-media simulation and transmission of EM waves in subwavelength split-ring-resonator-loaded metallic waveguides, Phys. Rev. Lett. 89 (2002) 183901.

[3] N. Katsarakis, G. Konstantinidis, A. Kostopoulos, R.S. Penciu, T.F. Gundogdu, M. Kafesaki, E.N. Economou, Th. Koschny, C.M. Soukoulis, Magnetic response of split-ring resonators in the far-infrared frequency regime, Opt. Lett. 30 (2005) 1348–1350.

[4] D.R. Smith, W.J. Padilla, D.C. Vier, S.C. Nemat-Nasser, S. Schultz, Composite medium with simultaneously negative permeability and permittivity, Phys. Rev. Lett. 84 (2000) 4184–4187.

[5] M. Bayindir, K. Aydin, E. Ozbay, P. Markos, C.M. Soukoulis, Transmission properties of composite metamaterials in free space, Appl. Phys. Lett. 81 (2002) 120–122.

[6] V.M. Shalaev, W. Cai, U.K. Chettiar, H. Yuan, A.K. Sarychev, V.P. Drachev, A.V. Kildishev, Negative index of refraction in optical metamaterials, Opt. Lett. 30 (2005) 3356–3358.

[7] J. Zhou, L. Zhang, G. Tuttle, T. Koschny, C.M. Soukoulis, Negative index materials using simple short wire pairs, Phys. Rev. B 73 (2006) 041101.

[8] J. Zhou, E.N. Economou, T. Koschny, C.M. Soukoulis, Unifying approach to left-handed material design, Opt. Lett. 31 (2006) 3620–3622.

[9] K. Guven, M.D. Caliskan, E. Ozbay, Experimental observation of left-handed transmission in a bilayer metamaterial under normal-to-plane propagation, Opt. Express 14 (2006) 8685–8693.

[10] G.V. Eleftheriades, L. Markley, A negative-refractive-index metamaterial for incident plane waves of arbitrary polarization, IEEE Anten. Wireless Propag. Lett. 6 (2006) 28–32.

[11] J. Zhou, T. Koschny, L. Zhang, G. Tuttle, C.M. Soukoulis, Experimental demonstration of negative index of refraction, Appl. Phys. Lett. 88 (2006) 221103.

[12] G. Donzelli, F. Capolino, A. Schuchinsky, Parametric analysis of electric and magnetic resonances in a metamaterial in planar technology, in: Proceedings URSI 2007, North American Radio Science Meeting, B-23, Ottawa, Canada, July 22–26, 2007, unpublished.

[13] J. Hao, Y. Yuan, L. Ran, T. Jiang, J.A. Kong, C.T. Chan, L. Zhou, Manipulating electromagnetic wave polarizations through anisotropic meta-materials, Phys. Rev. Lett. 99 (2007) 063908.

[14] G. Donzelli, F. Capolino, A. Schuchinsky, Anisotropic metamaterial in planar technology: phenomena, model, and particle resonances, in: Proceedings of Metamaterials 2007, First International Congress on Advanced Electromagnetic Materials in Microwaves and Optics, Rome, Italy, October 22–24, 2007, pp. 911–914.

[15] O.F. Siddiqui, M. Mojahedi, G.V. Eleftheriades, Periodically loaded transmission line with effective negative refractive index and negative group velocity, IEEE Trans. Anten. Propag. 51 (2003) 2619–2625.

[16] K. Aydin, K. Guven, C.M. Soukoulis, E. Ozbay, Observation of negative refraction and negative phase velocity in left-handed metamaterials, Appl. Phys. Lett. 86 (2005) 124102.

[17] C. Simovski, Bloch material parameters of magneto-dielectric metamaterials and the concept of Bloch lattices, Metamaterials 1 (2007) 62–80.

[18] J. Brown, Artificial dielectrics having refractive indices less than unity, Proc. Inst. Elect. Eng. 100 (1953) 51–62.

[19] R.N. Bracewell, Analogues of an ionized medium: applications to the ionosphere, Wireless Engr. 31 (1954) 320–326.

[20] W. Rotman, Plasma simulation by artificial dielectrics and parallel plate media, IRE Trans. Anten. Propag. 10 (1962) 82–95.

[21] J.B. Pendry, A.J. Holden, W.J. Stewart, I. Youngs, Extremely low frequency plasmons in metallic mesostructures, Phys. Rev. Lett. 76 (1996) 4773–4776.

[22] D.F. Sievenpiper, M.E. Sickmiller, E. Yablonovitch, 3-D wire mesh photonic crystals, Phys. Rev. Lett. 76 (1996) 2480–2483.

[23] J.B. Pendry, A.J. Holden, D.J. Robbins, W.J. Stewart, Low frequency plasmons in thin-wire structures, J. Phys.: Condens. Matter 10 (1998) 4785–4809.

[24] P.A. Belov, S.A. Tretyakov, A.J. Viitanen, Dispersion and reflection properties of artificial media formed by regular lattices of ideally conducting wires, J. Electromag. Waves Appl. 16 (2002) 1153–1170.

[25] P.A. Belov, R. Marqués, S.I. Maslovski, M. Silveirinha, C.R. Simovski, S.A. Tretyakov, Strong spatial dispersion in wire media in the very large wavelength limit, Phys. Rev. B 67 (2003) 113103.

[26] C.R. Simovski, P.A. Belov, Low-frequency spatial dispersion in wire media, Phys. Rev. E 70 (2004) 046616.

[27] M. Gorkunov, M. Lapine, E. Shamonina, K.H. Ringhofer, Effective magnetic properties of a composite material with circular conductive elements, Eur. Phys. J. B 28 (2002) 263–269.

[28] S. Zhang, W. Fan, N.C. Panoiu, K.J. Malloy, R.M. Osgood, S.R.J. Brueck, Experimental demonstration of near-infrared negative-index metamaterials, Phys. Rev. Lett. 95 (2005) 137404.

[29] S. Zhang, W. Fan, K.J. Malloy, S. Brueck, N.C. Panoiu, R.M. Osgood, Nearinfrared double negative metamaterials, Opt. Express 13 (2005) 4922–4930.

[30] G. Dolling, C. Enkrich, M. Wegener, C.M. Soukoulis, S. Linden, Low-loss negativeindex metamaterial at telecommunication wavelengths, Opt. Lett. 31 (2006) 1800–1802.

[31] G. Dolling, M. Wegener, C.M. Soukoulis, S. Linden, Design-related losses of double-fishnet negative-index photonic metamaterials, Opt. Express 15 (2007) 11 536–11 541.

[32] M. Kafesaki, I. Tsiapa, N. Katsarakis, T. Koschny, C.M. Soukoulis, E.N. Economou, Left-handed metamaterials: the fishnet structure and its variations, Phys. Rev. B 75 (2007) 235114.

[33] A. Vallecchi, F. Capolino, A.G. Schuchinsky, 2-D isotropic effective negative refractive index metamaterial in planar technology, IEEE Microw. Wireless Comp. Lett. 19 (2009), in press.

[34] B.A. Munk, Frequency Selective Surfaces: Theory and Design, John Wiley & Sons Inc., New York, 2004.

[35] D.M. Pozar, Microwave Engineering, 3rd ed., John Wiley & Sons Inc., 2005.

[36] M.A.R. Gunston, Microwave Transmission Line Impedance Data, Van Nostrand, New York, 1972.